Automation in Construction 143 (2022) 104588

Contents lists available at ScienceDirect

Automation in Construction

journal homepage: www.elsevier.com/locate/autcon

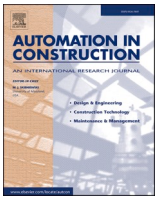

Structural grammar for design optimization of grid shell structures and diagrid tall buildings

V. Tomei [a,*], D. Faiella [b], F. Cascone [c], E. Mele [b]

[a] Department of Civil and Mechanical Engineering, University of Cassino and Southern Lazio, via G. Di Biasio 43, 00143 Cassino, Italy
[b] Department of Structures for Engineering and Architecture (DiST), University of Naples Federico II, Naples 80125, Italy
[c] AKT II, London EC1Y8AF, United Kingdom

ARTICLE INFO

Keywords:
Large structures
Grid shell
Diagrid
Structural grammar
Generative design
Structural optimization
Genetic algorithms
Steel structures

ABSTRACT

A great attention has been recently paid to sustainability and efficiency in the field of civil engineering. In this context, structural optimization processes combined with shape grammar constitute an important tool to support the design phase of large scale structures. This paper proposes shape grammars for the topology optimization of grid shells and diagrid tall buildings characterized by triangulated patterns, with the aim to minimize the structural weight. The structural feasibility of the generated solutions is assessed through numerical analyses, while the optimized patterns are identified by means of optimization processes based on genetic algorithm. The results are provided in terms of optimal geometrical patterns, structural weight, stiffness/strength checks. The approach is helpful to support the investigation of lightweight structural patterns and structurally efficient solutions. The method could be expanded and improved by considering the minimization of different objective functions that take into account both the weight and construction aspects.

1. Introduction

In the last few decades, a great attention has been paid to sustainability and efficiency in the architecture, engineering, and construction (AEC) industry. In the field of structural engineering, design strategies based on optimization techniques are being widely utilized by designers [1–6] and studied by researchers [7–20]. Often, structural optimization processes are thought to minimize the weight, the compliance, or in a more complex way, the cost, by fixing a given amount of material and boundary conditions, while ensuring that the constraint conditions imposed on structural performance are respected. Structural optimization techniques could be mainly divided into three categories, according to the variables of the problem [21]: sizing optimization, shape optimization and topology optimization. Sizing optimization assumes cross-sectional dimensions as variables, while the geometry and the topology are established a priori. In shape optimization the variable is the geometry of the structure, with topology set a priori. Finally, in topology optimization the variables define the connectivity of the nodes in the structure and/or the existence or absence of structural elements/parts [21]. This classification of the optimization problems suggests that the breadth of exploration, i.e. the design space, is related to the number of solutions potentially obtainable starting from the space of the design variables. For this reason, it is of paramount importance to combine structural optimization approaches with generative design processes, able to guarantee a wide space of design exploration. Among generative processes, an approach conceived many years ago [22], but re-evaluated in recent years [26–31] thanks to computational advancements, is shape grammar. A shape grammar is an algorithm composed by intertwined rules able to define a theoretical infinite number of potential solutions, unexpected in the phase of algorithm writing, starting from the definition of the design variables. In analogy to the grammar of language, the variables represent the words, which, combined through simple grammar rules, can give rise to an infinite number of sentences. This approach has been recently applied in different fields of architecture/engineering: Boonstra et al. [27] proposes a shape grammar-based method for the design of steel buildings: starting from the global dimensions of the structure, the method selects the most appropriate structural components (frame, truss, slab) in order to obtain the best configuration in terms of strain deformation energy; Mandow et al. [29] present an application of shape grammars for the generation of architectural sketches of small single-family dwellings, in order to find the distribution of spaces and openings that optimizes the energy consumption; Wang et al. [30] proposes shape grammars to support urban planning; Yu et al. [31] implemented a shape grammar for the

* Corresponding author.
E-mail addresses: v.tomei@unicas.it (V. Tomei), diana.faiella@unina.it (D. Faiella), elenmele@unina.it (E. Mele).

https://doi.org/10.1016/j.autcon.2022.104588
Received 11 July 2022; Received in revised form 9 September 2022; Accepted 16 September 2022
Available online 23 September 2022

generation of Origami patterns, to be used for structural purposes.

In the field of structural engineering, the shape grammar supports the definition of geometrical models, but it is agnostic of the structural behaviour, which, however, is fundamental to evaluate the structural feasibility of the generated solutions; therefore, structural models should be created for each solution generated by the shape grammar process, and analyses should be carried out under design loads. The combination of shape grammar, structural analysis and optimization processes gives rise to the so-called structural grammar [22–25], which represents a successful approach in the search for optimal design solutions. In this context, the present paper proposes structural grammars for the generative design of triangulated mega-structures representing paradigmatic cases where the choice of the pattern also affects geometry, architectural features, and constructive aspects.

The mega-structures here referred to are grid shells and diagrids, namely long span and high rise buildings characterized by a grid, or pattern, of structural members arranged to form triangles.

Diagrid structures have emerged in the last two decades as one of the most popular lateral load resisting systems for tall buildings [32,33], which has also sparked the interest of the scientific community [9,16,34–45]. Diagrid tall buildings are constituted by a triangulated pattern covering the whole building façades; the grid of diagonal members is characterized by inherently high rigidity, particularly important since tall buildings' design is often governed by the limitation of the lateral drift and building motion. Recent works have highlighted the major role of the diagonal slope on the structural performances of diagrid tall buildings, suggesting that the optimal angle value increases with the building slenderness [7,46–48] and that design solutions with variable angles along the elevation and/or the width are more efficient than uniform-angle configurations for very slender buildings [46,47]. This trend turns out to be intuitive by considering the analogy between the tall building and the vertical cantilever beam under lateral load [3,7,9]. However, in the case of buildings with low slenderness, the stiffness capacity provided by the triangulated pattern may exceed the stiffness demand, and the member sizing may be governed strength demand [8,16]. The structural grammar proposed by the authors for diagrid tall buildings is able to find the optimized pattern by changing the number and slope of diagonals both along elevation and width, as well as to take into account the different stiffness and strength demands varying the slenderness of the building.

Grid shells structures, widely used as canopies for long-span public buildings, are widely used for their capacity to cover large spans with light solutions, exploiting the inherent rigidity of double-curvature shells. The characteristic of lightness, typical of grid shells, could be further improved through design optimization strategies. In this context, different approaches are proposed in literature, which consider as variable the topology [49,50], the shape [51,52], or the node rigidity [53]; other proposals combine some of these approaches with sizing optimization [17–20,54–57]. The actual trend to design free-form grid shells [58–60] enhances the importance of optimizing the structural pattern, which strongly affects the structural behaviour [61]. The structural grammar for the design of grid shell structures presented in this paper is able to optimize the topology of the pattern, by varying number and position of the structural elements, for shells characterized by different global shape.

In the following, detailed descriptions of the two structural grammars are provided. The grammars are applied to tall building and grid shell models characterized by different geometry and the optimal patterns are obtained. All the results are provided in terms of structural pattern, structural weight and stiffness/strength checks for both grid shells and diagrids. The optimal solutions are derived for structures characterized by different values of the aspect ratio (ratio between the height of the structure and the base dimension), a parameter that in both cases strongly affects the structural behaviour.

2. Structural grammars for the generation of optimized patterns

The structural grammar proposed for the topology optimization of grid shell structures and diagrid tall buildings is schematically described in the flow chart of Fig. 1. In particular, the flow chart is divided into shape grammar, devoted to the definition of the geometry (Fig. 1 - box a), structural modeling and analysis (Fig. 1 - box b and c), and topology optimization (Fig. 1 - box d), which drives the search of the optimal solution. More in details, the shape grammar (box a) is able to define a multitude of geometrical patterns starting from few parameters that govern the distances between the intersection points of the structural members. It is divided into two phases: the first one is devoted to the definition of the design domain; the second one is devoted to the discretization of the design domain by defining the number and position of structural members on the base of the parameters which govern the distances between nodes – i.e. it defines the structural pattern. Then, each generated solution is assembled in a structural model (Fig. 1 - box b), which structural elements are sized with an iterative process that confers the smallest possible cross-sections able to meet the stiffness and strength requirements (Fig. 1 - box c); for each solution, the structural weight and the structural performances are evaluated, and the fitness function (the structural weight, in this specific case), is recorded. Hence, the topology optimization process – based on genetic algorithms [62] – analyses the fitness values of each solution, and drives the search for the optimal one (i.e. the solution that minimizes the weight), by varying the parameters of the shape grammar (Fig. 1 - box d). While the phases of structural design (Fig. 1 - box c) and topology optimization (Fig. 1 - box d) are almost the same for grid shells and diagrids, the shape grammar for the two structural systems is different: in subsequent sections, all phases of the structural grammar are described in details highlighting similarities and differences.

The structural grammar has been developed within the Grasshopper environment [63,64], a Rhinoceros [64] plug-in for the algorithmic-aided design based on visual scripting. The structural analyses are carried out through Karamba [65,66], a Grasshopper plug-in for finite element analyses [63,64].

3. The shape grammar

The shape grammar consists of three types of rules: rules for the

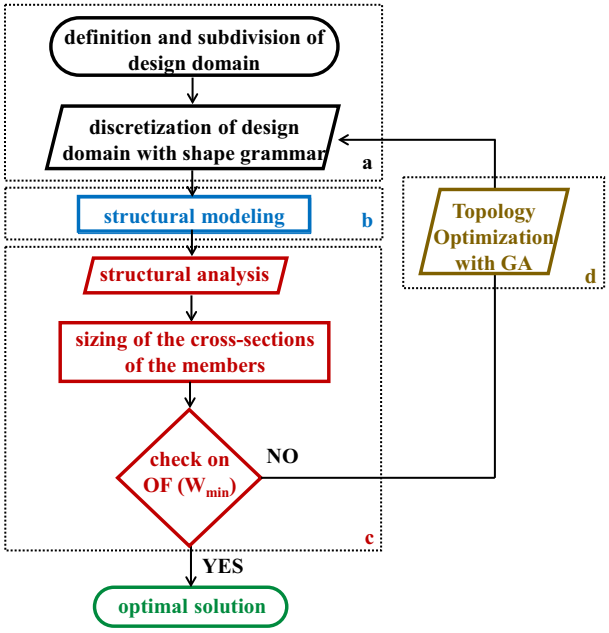

Fig. 1. Flowchart of the structural grammar.

definition of the design domain, rules for the discretization of the design domain, and rules for the definition of the pattern. The design domain identifies the volume occupied by the model, which mainly depends on the structural geometry, namely the plan width B and the height H of the grid shell or the diagrid façade (Fig. 2). The discretization of the design domain is based on the definition of a "structural unit" that is repeated several times to build the pattern. In the grid shell, the structural unit is the shell sector shown in Fig. 2a, i.e. the structural portion corresponding to the one eight slice of shell that, mirrored seven times, gives rise to the entire grid shell. For the building diagrid, instead, the structural unit is a quarter of a module (Fig. 2b); the module, in turn, is the horizontal fascia covering the full width of the building façade and spanning multiple floors. The diagrid's façade is conceived by subdividing its elevation into three macro-modules, each consisting of a certain number of modules with the same geometrical characteristics. The quarter of module (i.e., the structural unit) is mirrored three times to obtain the whole module and replicated along elevation until covering the height of the macro-module.

3.1. Rules for the definition of the design domain

The Rules type 1 concerns the definition of the design domain (Fig. 3), i.e. the volume occupied by the structural model, for both grid shell and diagrid.

For the grid shell, the footprint in plan is characterized by a quadrangular shape with dimensions B x B set a priori, on which nine control points are defined, eight along the perimeter and one in the middle of the square (point c(H) in Fig. 3). The Rule 1.1 defines the height H of the control point c(H) and the Rule 1.2 defines the three-dimensional shape of the model by the construction of a NURBS (Non Uniform Rational Basis Splines) surface that passes through the nine control points. In this study, different surfaces are generated and analysed by varying the height H, thus giving rise to models characterized by different rise - span ratios H/B.

Analogously, for the diagrid the footprint in plan is defined by a quadrangular base surface – Rule 1.1 – with dimensions B x B. The Rule 1.2 replicates the quadrangular surface along elevation, until covering the height of the building. Differently from the grid shell, in addition to the width B and the height H of the building's façade, other geometrical parameters are introduced for subdividing the design domain along elevation, namely: inter-storey height, h_s; number of macro-modules, n_M; number of modules for each macro-module, n_{mj} with $j = 1, \ldots, n_M$; total number of modules in the pattern, $n_m = \Sigma_j\, n_{mj}$. In this study, the width B and the inter-story height h_s are fixed a priori, while the number of macro-modules n_M, of modules in each macro-module n_{mj}, and, in turn, of the total modules n_m, vary to generate building models characterized by different slenderness ratios H/B.

3.2. Rules for the discretization of the design domain

For both grid shell and diagrid, the discretization of the domain is obtained by applying the Rules type 2 (Fig. 4), starting from the definition of the distances between the nodes of the structural unit (i.e. the sector for the grid shell and one quarter of module for the diagrid, see Fig. 2), which control the structure's topology. The main difference in the formulation of the rules for the grid shell and the diagrid concerns the nodes' range of movement, since for the grid shell's sector it is along both x and y directions while for the diagrid's one quarter of module movement is only allowed along x direction.

3.2.1. Grid shell discretization

Considering the grid shell, the Rule 2.1 identifies the plan projection of one sector of the NURBS surface in normalized local coordinates (x, y), whose origin is defined with respect to the global coordinate system (X, Y), as:

$$x = \frac{X + \frac{B}{2}}{B};\ y = \frac{Y}{B} \tag{1}$$

The Rule 2.2 defines the position of the starting nodes $P_{st,i}(x_{st,i}, y_{st,i})$ (with $i = 1, \ldots, n_n$, with n_n the number of the sector nodes) of the sector, initially spaced at 0.1 of the normalized dimension of the domain in both directions, i.e. 0.1B. Considering that the two catheti of the triangular sector are both equal to 0.5B and the starting nodes are placed at 0.1B, the number of the starting nodes n_n is equal to 21. The Rule 2.3 creates lines between points, thus defining the node connectivity. The Rule 2.4 defines the range of movement of the sector's nodes by means of sliders that control the distance along the directions x, a_{xi}, and y, a_{yi}, with respect to the position of the relevant starting node $P_{st,i}(x_{st,i}, y_{st,i})$, where the parameters a_{xi} and a_{yi} are given by:

$$-0.1 = a_{x,min} \le a_{x,i} \le a_{x,max} = 0.1 - 0.1 = a_{y,min} \le a_{y,i} \le a_{y,max} = 0.1 \tag{2}$$

with minimum and maximum values respectively equal to $a_{x,min}$, $a_{x,max}$, $a_{y,min}$, and $a_{y,max}$.

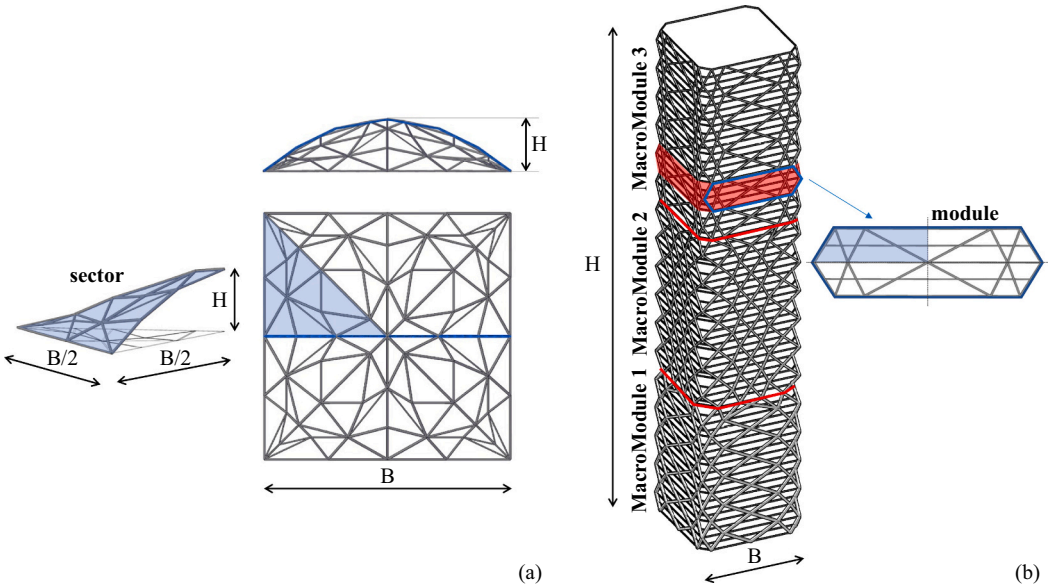

Fig. 2. Global geometry and structural unit: (a) grid shell, (b) diagrid.

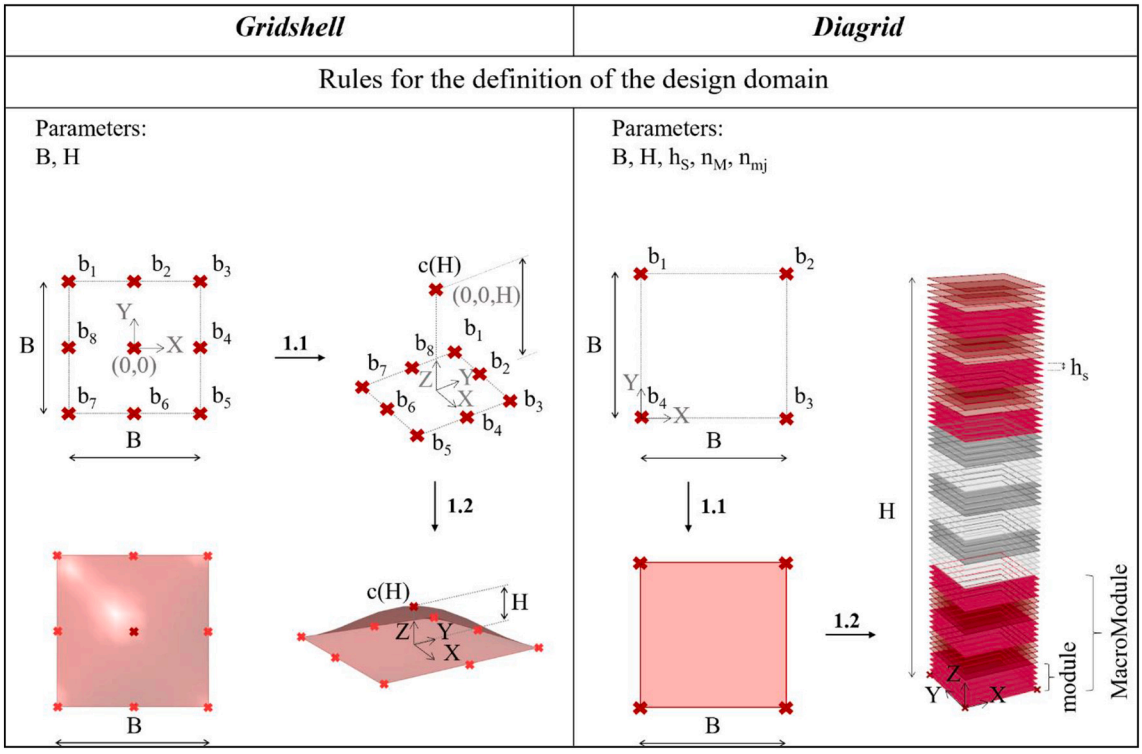

Fig. 3. Rules for the definition of the design domain.

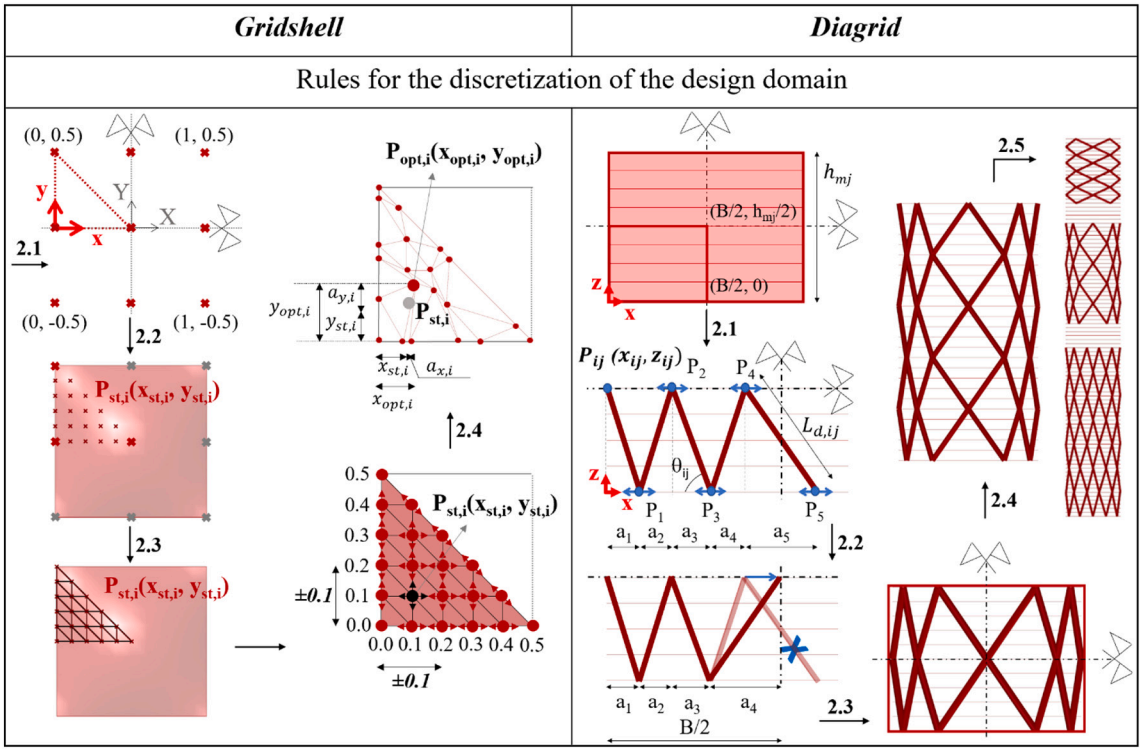

Fig. 4. Rules for the discretization of the design domain.

In particular, each node reaches the optimal position at the point $P_{opt,I}$ ($x_{opt,i}$, $y_{opt,i}$) of coordinates defined as:

$$x_{opt,i} = x_{st,i} + a_{x,i}$$
$$y_{opt,i} = y_{st,i} + a_{y,i} \quad (3)$$

Further rules are defined for the variables $a_{x,i}$ and $a_{y,i}$ to ensure that the edge points remain along the sector's perimeter after the optimization process. These rules are defined as:

$$a_{x,i} = 0 \text{ If } x_{st,i} = 0 \text{ and } y_{st,i} \neq 0 \quad (4)$$

$$a_{y,i} = 0 \text{ If } x_{st,i} \neq 0 \text{ and } y_{st,i} = 0 \quad (5)$$

$$a_{x,i} = a_{y,i} = 0 \text{ If } \left(x_{st,i} = 0, y_{st,i} = 0\right) \text{ or } \left(x_{st,i} = 0.5, y_{st,i} = 0\right) \text{ or } \left(x_{st,i} = 0, y_{st,i} = 0.5\right) \quad (6)$$

$$a_{x,i} = -a_{y,i} \text{ If } x_{st,i} + y_{st,i} = 0.5 \text{ and } x_{st,i} \neq 0 \& y_{st,i} \neq 0 \quad (7)$$

Taking into account the right-angle triangle formed by the plan projection of the shell sector, the rules in Eqs. (4) and (5) allow nodes with zero abscissa or zero ordinate to move only along the y or x cathetus, respectively; the rule in Eq. (6) maintains fixed the vertices of the triangle; the rule in Eq. (7) allows the nodes on the hypotenuse to move only along it.

3.2.2. Diagrid discretization

The discretization of the diagrid single module is defined by diagonals that create a sequence of rhombuses, made by means of two triangular units, superimposed base to base (Fig. 4). More in detail, the algorithm starts from the definition of the diagonals in one quarter of module that, mirrored with respect the two axes of symmetry, creates the whole module. Then, the discretization of the relevant macro-module is obtained by replicating the module along elevation. The number and slope of diagonals within a module are established starting from the parameters a_{ij} of Fig. 4 (Rule 2.1), which define the horizontal distance between the two points that work as sliders, i.e. the end points of the *i-th* diagonal within the generic module of the *j-th* macro-module. The algorithm generates the geometry of the quarter of module by varying the parameters a_{ij}, so that, by considering a local coordinate system (x, z) with the origin at the lower left corner of the module, the diagonal's end points P_{ij} (x_{ij}, z_{ij}) are defined by the coordinates:

$$x_{ij} = \sum_{i=1}^{k} a_{ij} \; z_{ij} = \left\{ \begin{array}{c} \frac{h_{mj}}{2} \text{ for even numbers} \\ 0 \text{ for odd numbers} \end{array} \right\} \quad (8)$$

with

$$a_{ij} = x_{ij} - x_{i-1,j} \quad (9)$$

$k \leq n_{dj}/2$

n_{dj} the number of diagonals in the quarter of the module of the *j-th* macro-module,

h_{mj} the height of the same module.

The point at the module's upper left edge is not a slider, since it is fixed at local coordinates (0, $h_{mj}/2$). Given the values of the parameter a_{ij}, the slope θ_{ij} and the length $L_{d,ij}$ of the *i-th* diagonal of the *j-th* macro-module are defined as:

$$\theta_{ij} = tan^{-1}\left(\frac{h_{mj}}{2a_{ij}}\right) \; L_{d,ij} = \frac{a_{ij}}{cos\left(tan^{-1}\left(\frac{h_{mj}}{2a_{ij}}\right)\right)} \quad (10)$$

The Rule 2.2 controls the number of diagonals n_{dj} in the quarter of module, imposing that no diagonal crosses the half-width line of the building façade. This is equivalent to set the sum of the distances a_{ij} ($\sum_{i=1}^{n_{dj}} a_{ij}$) exactly equal to B/2, i.e. the abscissa of the end point of the innermost diagonal should be exactly equal to B/2; therefore, if it is greater than B/2, the Rule 2.3 deletes the innermost diagonal and moves the end point of the previous diagonal until reaching $x_{ij} = B/2$.

Within the *j-th* macro-module, the variation's range of the parameters a_{ij} depends on the ranges set for the number n_{dj} and for the slope θ_{ij} of diagonals. In this context, considering that θ_{ij} should vary between a minimum and maximum value ($\theta_{ij,min} = 45°$ and $\theta_{ij,max} = 85°$), and that the module height h_{mj} and number of storeys in the single module $n_{s,m}$ are fixed (here, $n_{s,m} = 4$), the range of variation of a_{ij} can be obtained as a function of $\theta_{ij,max}$ and $\theta_{ij,min}$, and of h_{mj}, i.e.:

$$a_{ij,min} = \frac{h_{mj}}{2 \bullet tan\left(\theta_{ij,max}\right)} \leq a_{ij} \leq a_{ij,max} = \frac{h_{mj}}{2 \bullet tan\left(\theta_{ij,min}\right)} \quad (11)$$

where $h_{mj} = h_s \; n_{s,\,m}$.

Quite trivially, the range of a_{ij} also controls the range for the number n_{dj} of diagonals: $\frac{B}{a_{ij,max}} \leq n_{dj} \leq \frac{B}{a_{ij,min}}$.

Once the discretization of the quarter of module is done, the relevant diagonals are mirrored once with respect to the vertical axis, and once with respect to the horizontal axis, to generate the entire module (Rule 2.3), which is then replicated along elevation until covering the height of the relevant macro-module (Rule 2.4). Finally, the Rule 2.5 disposes all macro-modules along elevation.

3.3. Rules for the definition of the pattern

The discretization of the design domain is defined according to the rules illustrated in the previous section, but some adjustments are necessary to make the solutions feasible from a constructive point of view. It is worth underlining that these rules depend on the specific structural system, hence they are different for the grid shell and diagrid structures (Fig. 5). For the former, Rules 3 control the distance between points in the sector that, in turn, is mirrored to build the entire structural pattern. For the latter, the entire structural pattern is obtained by applying the Rules 3, that connect the diagonals' end points of two stacked macro-modules, and the Rule 4.1, that chamfers the building corners also according to the bird mouth profile, typical of diagrid buildings (e.g. Hearst Tower).

More in detail, for the grid shell, the nodes' range of movement can cause some nodes to be almost coincident or very close to each other, leading to unfeasible solutions due to the small angles between the members. To solve this issue, Rule 3.1 overlaps very close points (at a distance lower than a specific value, set equal to 2 m in this study) and deletes coincident points; these pattern adjustments affect the number of nodes and members, which therefore may change during the generation of geometries. It means that, starting from the position of points $P_{opt,i}(x_{opt,i}, y_{opt,i})$ directly obtained by the optimization process, the position of the final points $P_i(X_i, Y_i, Z_i)$ in the global coordinate system (X, Y, Z) is derived so that the distance of two successive points is >2 m. As an example in Fig. 5, by considering the points P_A (X_A, Y_A, Z_A) and P_B (X_B, Y_B, Z_B), it should be verified that:

$$\sqrt{(X_B - X_A)^2 + (Y_B - Y_A)^2 + (Z_B - Z_A)^2} \leq 2 \text{ m} \quad (12)$$

Then, the geometry and the discretization of the shell sector is mirrored with respects the axes of symmetry (Fig. 5) to obtain the whole structural pattern.

As regards the diagrid, since the module geometry may change from one macro-module to another one, the diagonals' end points at the interface between two consecutive macro-modules may not coincides. To overcome this problem, stacking macro-modules are not directly connected, but a transition belt is created between them. In particular, Rule 3.1 identifies the end points of the macro-modules that should be connected, i.e. the points with maximum ordinate of the lower macro-module and the points of minimum ordinate of the upper one. Rules 3.2 and 3.3 respectively joins overlapped and staggered points in the half width of the upper and lower macro-modules, going from the edge to the middle of macro-module. Then, Rule 3.4 mirrors the diagonals with respect the vertical axis of symmetry, to cover the entire width of the building. A further rule (Rule 4.1) is introduced to build the tapered chamfering of the building corner, which accommodates the triangulated pattern. At this point, the geometrical definition of the diagrid tall building is completed.

It is interesting to highlight that the shape grammar, although it regulates the geometry of the model and is not aware of the structural behaviour, is capable of generating configurations that can be realized

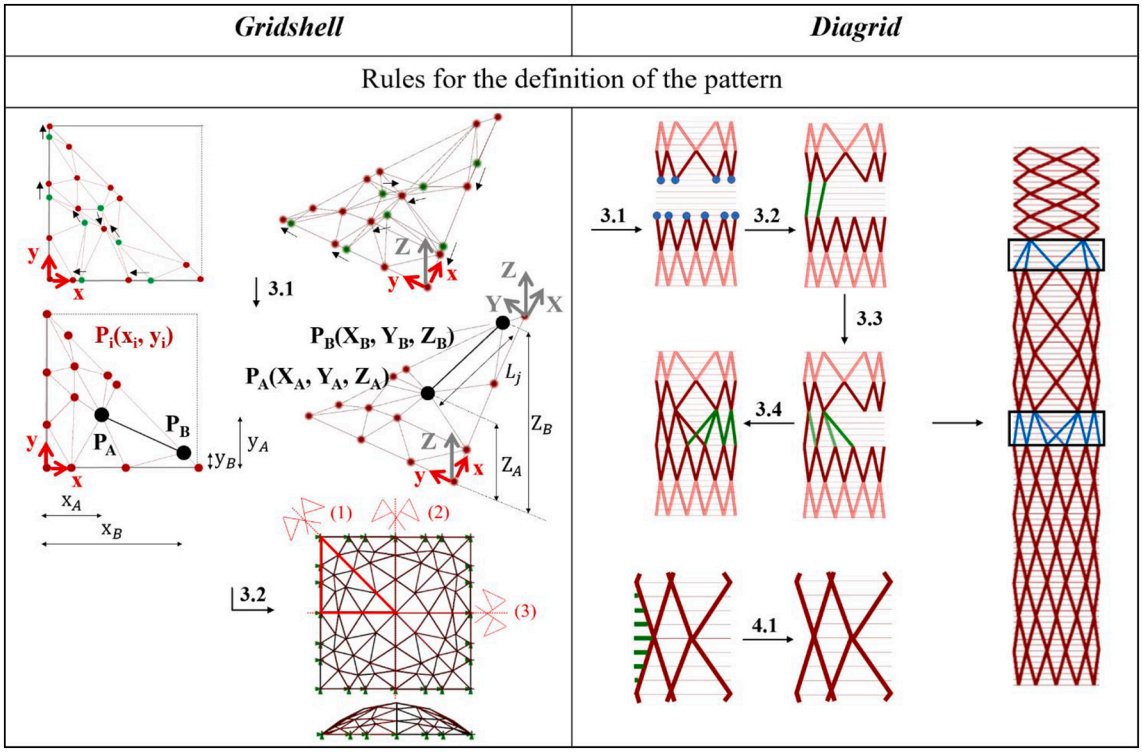

Fig. 5. Rules for the definition of the pattern.

from a structural point of view, thanks to the constraints on the maximum distance between nodes in grid shell and to the generation of the transition belt and chamfered building corners in diagrid.

4. Structural models, member sizing and pattern optimization

Once the geometrical models of the gridshell and diagrid have been defined through the relevant shape grammars, the structural models are created, designed in terms of member cross-sections, and analysed by means of the Finite Element code Karamba [65,66]. In this study, the grid shell models are characterized by dimensions of the base quadrangular plan B of 24 m, and by three values of rise to span ratio, H/B, equal to 0.00, 0.21, 0.42, respectively; the diagrid models are characterized by base B equal to 54 m, and by three values of aspect ratio H/B equal to 3, 5, 6.6. The structural material used for both grid shell and diagrid is steel S275 (f_{yk} = 275 MPa).

From the modeling point of view, the structural members are represented by beam elements perfectly clamped to each other. The full restraint at the ends of members is particular influential in the response of the grid shells, since by varying the rise-to-span ratio, the magnitude of bending moment in the members varies. On the other hand, in case of diagrid, the members work predominantly in the axial direction.

In addition to the structural weight, two levels of superimposed loads q are considered for assessing the effect of increasing vertical loads on the grid shell's performances, i.e. q = 3.5 kN/m^2 and q = 10 kN/m^2. For the diagrid, the design gravity loads are given by dead load of 7 kN/m^2 and live load of 4 kN/m^2; the lateral loads due to the wind pressure are computed according to Eurocode 1 (EN 1991–1, 2010) [67] by considering a wind speed of 50 m/s, which provides the following values of global overturning moment and base shear: 2585 MNm and 29 MN for H/B = 3; 8171 MNm and 54 MN for H/B = 5; and 13,043 MNm and 69 MN for H/B = 6.6.

Constraint conditions are imposed to translate local strength requirements (members' Demand to Capacity Ratio DCR ≤ 1, where DCR accounts for axial stresses, local buckling, bending and shear stresses) and global stiffness requirements (maximum displacement D_{max} ≤ limit displacement D_{lim}). In particular the DCR is evaluated as:

$$DCR = max\begin{cases} DCR_b = \begin{cases} if\ N > 0: \dfrac{N}{N_{Rd}} + \left|\dfrac{M_y}{M_{y,Rd}}\right| + \left|\dfrac{M_z}{M_{z,Rd}}\right| \\ if\ N < 0: -\dfrac{N}{N_{b,Rd}} + \left|\dfrac{M_y}{M_{y,Rd}}\right| + \left|\dfrac{M_z}{M_{z,Rd}}\right| \end{cases} \\ DCR_s = \left|\dfrac{S}{S_{y,Rd}}\right| + \left|\dfrac{S_z}{S_{z,Rd}}\right| \end{cases} \quad (13)$$

DCR_b is the Demand to Capacity Ratio evaluated for normal forces and bending moments, where: N is the normal force, which is positive for tension and negative for compression; N_{Rd} is the resisting normal force; $N_{b,Rd}$ is the buckling force, evaluated as suggested in Eurocode 3 [68]; M_y and M_z are the bending moments evaluated along the local y and z axis of the members (Fig. 6), respectively; $M_{y,Rd}$ and $M_{z,Rd}$ are the resisting bending moments evaluated along the local y and z axis of the members (Fig. 6), respectively; DCR_s is the Demand to Capacity Ratio evaluated for shear forces, where S_y and S_z are the shear forces acting along the local y and z axis of the members (Fig. 6), respectively; $S_{y,Rd}$ and $S_{z,Rd}$ are the shear forces evaluated along the local y and z axis of the members (Fig. 6), respectively.

For the grid shell, the maximum displacement D_{max} refers to the maximum vertical displacement; two different values for the limit displacement are assumed in this study, i.e. D_{lim} = B/250 and D_{lim} = B/500. For the diagrid, D_{max} refers to the top horizontal displacement of the building, while D_{lim} is assumed equal to H/500. The process of structural members' sizing is the same for grid shell and diagrid and consists of an iterative design process, as implemented in the Optimize Cross Section component of Karamba [65,69]. The iterative process

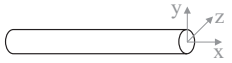

Fig. 6. Local axis of structural members.

selects, for groups of structural elements previously defined by the user, the smallest cross section within a set of user-defined cross sections that guarantees the strength/stability requirement (evaluated in terms of DCR). At the end of the process, the stiffness requirement is checked and, if not verified, some adjustments are made to cross-sections, until reaching $D_{max} \leq D_{lim}$.

The last phase of the proposed structural grammar concerns the pattern optimization, which involves all the previous phases. This phase, indeed, drives the generation of the patterns, by varying the parameters of the shape grammar (Section 3), and selects the optimal one in terms of weight, by means of a Topology Optimization process that involves genetic algorithms. Each generated solution is sized in terms of cross-sections and evaluated in terms of weight and structural performances (Section 4) by the optimization algorithms.

The optimization problem is defined in Table 1; for both grid shell and diagrid, the objective is to minimize the weight W. The grid shell and diagrid solutions are made of steel structural material, with a steel weight γ_s. For the grid shell, L and A are the length and cross-section area of the generic member, n_{int} is the number of members placed within the sectors, n_{edge} is the number of members on the grid shell edge, n_c is the number of members on the common sides of two adjacent sectors, the subscripts i, j, k vary within the following ranges: $i = 1, \ldots, n_{int}$, $j = 1, \ldots, n_{edge}$, $k = 1, \ldots, n_c$. For the diagrid, n_M is the macro-modules' number, n_{mj} is the modules' number in the *j-th* macro-module, $L_{d,ij}$ and A_{ij} are the length and cross-section area of the *i-th* diagonal, n_{dj} is the number of diagonals along the width of the module. For the grid shell, the variables are the horizontal and vertical distances $a_{x,i}$ and $a_{y,i}$ between initial and final position of the nodes; for the diagrid, the variables are the horizontal distances between the end nodes of diagonals a_{ij}. For both grid shell and diagrid, constraint conditions are imposed on the design variables, as described in Section 3.1 and reported in Table 1.

The genetic algorithm [62] employed in these processes is Galapagos of Grasshopper, inspired to the principle of the natural selection [63]. The basic steps of the algorithm, which drives the search of the optimal solutions, depicted in Fig. 7, are:

1. generation of the first population (first generation) with random individuals, structural patterns, characterized by random values of $a_{x,i}$ and $a_{y,i}$ for the grid shell, and random values of a_{ij} for the diagrid;
2. computation of the fitness function (weight) for each individual of the current generation and ranking of the individuals according to their fitness value;
3. selection of the best individuals (the lightest ones) of the current generation that go directly to the next generation (Maintain); selection of the individuals to mate to obtain offsprings for the next generation (Crossover); selection of individuals subjected to random mutation for the next generation (Mutation);
4. creation of the new population;
5. repeat steps from 2 to 4, until no reduction of the fitness function is obtained for a specified number (50 in this paper) of generations.

The last point indicates that a threshold of 50 successive stagnant generations is employed as stopping criterion of the algorithms, where the terms "stagnant generations" indicates generations characterized by the same value of the objective function (accuracy of 2 decimal digits). As an example, Fig. 8 shows the convergence path for the grid shell characterized by a rise-to-span ratio H/B equal to 0.21 and subject to a load q equal to 3.5 kN/m^2.

Table 1
Optimization problem.

	Grid Shell	Diagrid
Minimize	$W = \gamma_s \bullet (\sum_{i=1}^{n_{int}} L_i A_i + \sum_{j=1}^{n_{edge}} L_j A_j + \sum_{k=1}^{n_c} L_k A_k)$	$W = \gamma_s \bullet 4 \bullet \sum_{j=1}^{n_M} n_{mj} \bullet 4 \bullet \sum_{i=1}^{n_{dj}/2} L_{d,ij} \bullet A_{ij}$
Variables	$a_{x,i}$; $a_{y,i}$ for $i = 1, \ldots, n_n$	$a_{ij} = \frac{h_s \bullet n_{s,mj}}{2 \bullet tan(\theta_{ij})}$ for $i = i, \ldots, n_{dj}/2$ and $j = 1, \ldots, n_M$
Constraints	$a_{x,min} \leq a_{x,i} \leq a_{x,max}$ $a_{y,min} \leq a_{y,i} \leq a_{y,max}$ for $i = 1, \ldots, n_n$	$a_{ij,min} \leq a_{ij} \leq a_{ij,max}$ for $i = i, \ldots, n_{dj}/2$ and $j = 1, \ldots, n_M$

5. Structural solutions and performance assessment

The optimal structural patterns are shown in Fig. 9, for both grid shells and diagrids.

The grid shells' cross-sections are depicted with an extruded view. For H/B = 0, i.e. for flat grid shells, solutions characterized by different geometries and number of structural elements are obtained under vertical loads q equal to 3.5 and 10 kN/m^2 (Fig. 9a and b respectively). In fact, the load intensity strongly affects the generation of the optimal patterns, and in particular the grid density. On the contrary, the optimal patterns obtained for H/B = 0.21 (Fig. 9c) and H/B = 0.42 (Fig. 9d) do not vary by changing the load intensity. Furthermore, they are characterized by smaller cross-sections with respect to the case of H/B = 0, as evident from the extruded view. These results confirm the different behaviour of the grid shell as a function of the ratio H/B, as will be discussed in the following.

Looking at the diagrid patterns, from Fig. 9e, f, g it can be observed that the diagonals are steeper and denser at the edges and become less inclined toward the centre of the building façade. The variable density of the grid allows to satisfy the different demands of axial strength due to overturning moment along the width of the building façade, and contemporarily to maximize the bending stiffness of the structure. Also in this case, the visual results of the patterns suggest a variation of the structural behaviour among models characterized by different slenderness ratios H/B [8]. As the slenderness increases, the optimal patterns become ever more similar to the trend of the isostatic lines, thus further improving the inherent efficiency of the diagrid [9].

The unit structural weight W/A (i.e. the ratio between the total weight of the structural steel utilized for the optimal pattern solution and the total floor area of the building), the maximum values of the DCR (DCR_{max}), the ratio D_{max}/D_{lim}, are provided in Fig. 10 and Fig. 11 for the grid shells and diagrids, respectively.

Looking at the optimal grid shell solutions (Fig. 10), for each ratio H/B the two vertical loads q of 3.5 and 10 kN/m^2, as well as the two limits of B/250 and B/500 are considered. In particular, for H/B = 0 it can be observed that the values of DCR_{max} are smaller than 0.7 while the values of D_{max}/D_{lim} reach the unity; therefore, it can be deduced that the design is dominated by the stiffness requirements and, quite trivially, the structural weight increases as D_{lim} decreases and q increases. Further, from Fig. 9a and b it also emerges that, for a given value of load q, the increase of stiffness demand due to the reduction of D_{lim} does not lead to a variation of the structural pattern, but it is satisfied by increasing the cross-section of the members, as shown by the increase of weight reported in Fig. 10; on the other hand, for a given value of D_{lim}, the increase of stiffness demand due to the increase of the external load q, is satisfied by varying the structural pattern, and in particular by increasing the number of structural elements. Conversely, for H/B equal to 0.21 and 0.42 the design is dominated by the strength requirements, thanks to the remarkable inherent stiffness of curved grid shells, as compared to flat counterparts. In fact, the values of DCR_{max} reach the unity and the values of D_{max}/D_{lim} are smaller than 0.7; the structural weight is independent on the limit displacement D_{lim}, while it slightly increases at increasing vertical load q as a consequent increment of larger members' cross-section. With specific reference to the analyses carried out, it is interesting to highlight that the structural weight (i.e. the members' cross sections) is particularly sensitive to the variation of the external loads q and the limit displacement D_{lim} only for the case H/B = 0; indeed, for low value of H/B, the structural members are forced to work in bending, while increasing H/B the members are mainly subject to axial forces rather than bending moments. Since the bending stiffness

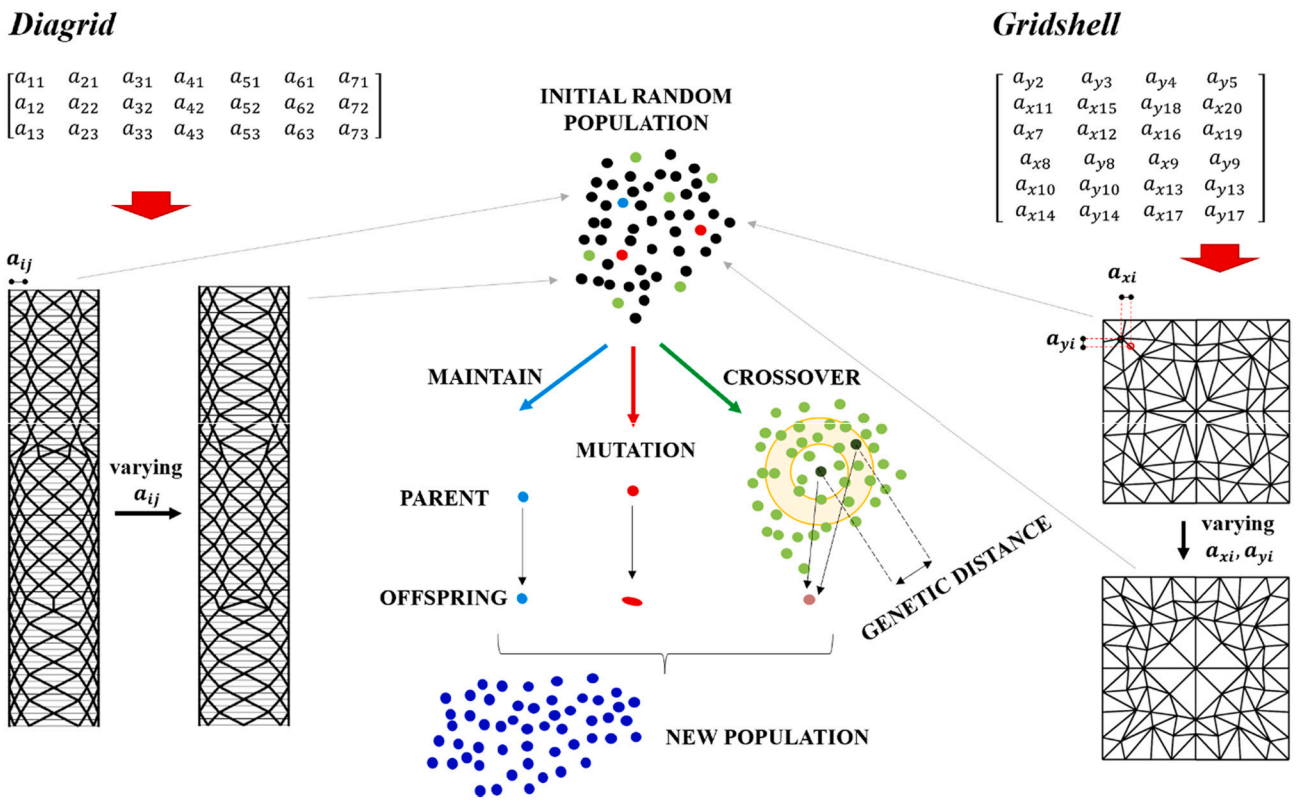

Fig. 7. Framework of the generation algorithm.

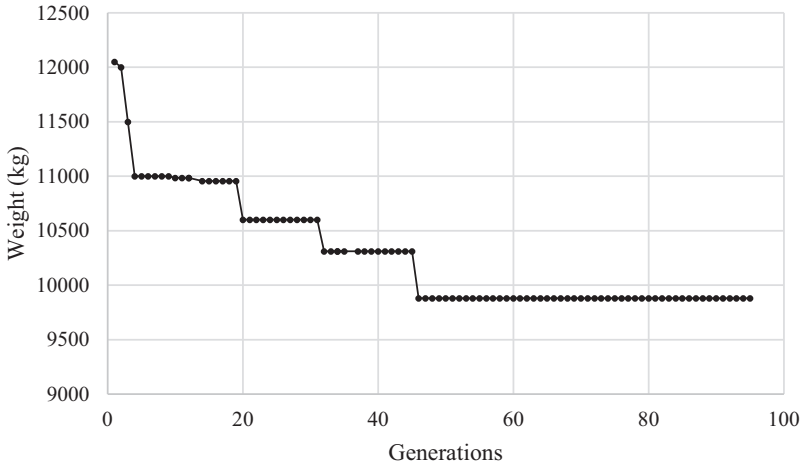

Fig. 8. Convergence path: grid shell, H/B = 0.21 and q = 3.5 kN/m^2.

of a slender beam is much less than its axial stiffness, it is clear that the increase of stiffness/ strength required due to higher external load has to be accommodated by a larger increase of cross-sections for bent members rather than for stretched members; further, when the vertical load q increases, an increase of cross-sections is not sufficient to guarantee an adequate level of stiffness; this, in turn, leads to the need of increasing the number of elements, i.e. to the variation of the structural pattern, driven by the optimization algorithm.

Considering the optimal diagrid solutions (Fig. 11), for the smallest aspect ratios the values of DCR_{max} approach the unit limit value, while the value of D_{max}/D_{lim} is smaller than one, equal to 0.4 and 0.7 for H/B equal to 3 and 5, respectively. On the contrary, for H/B = 6.6, the value of D_{max}/D_{lim} tends to the unity while DCR_{max} is close to 0.9. Therefore, the governing design criterion is strongly related to the aspect ratio of the building, as it affects the flexibility of the structure [8]. Indeed, for small aspect ratios, the intrinsic rigidity provided by the triangulated pattern is enough to satisfy the global stiffness requirements, consequently the design problem is governed by local strength requirements; instead, for high aspect ratios, the design problem is mainly dominated by stiffness requirements. In addition, as previously mentioned, by increasing the aspect ratios, the diagrid pattern becomes ever more similar to the trend of the isostatic lines [9].

Further, the unit structural weight W/A increases with the aspect ratio, as expected, according to the premium for height concept [32], but, unlike other structural systems that are characterized by a more-than-linear trend, in this case the premium for height is characterized by an almost linear increase of structural weight versus height. It means that the use of diagrid, in particular if it is designed with the proposed

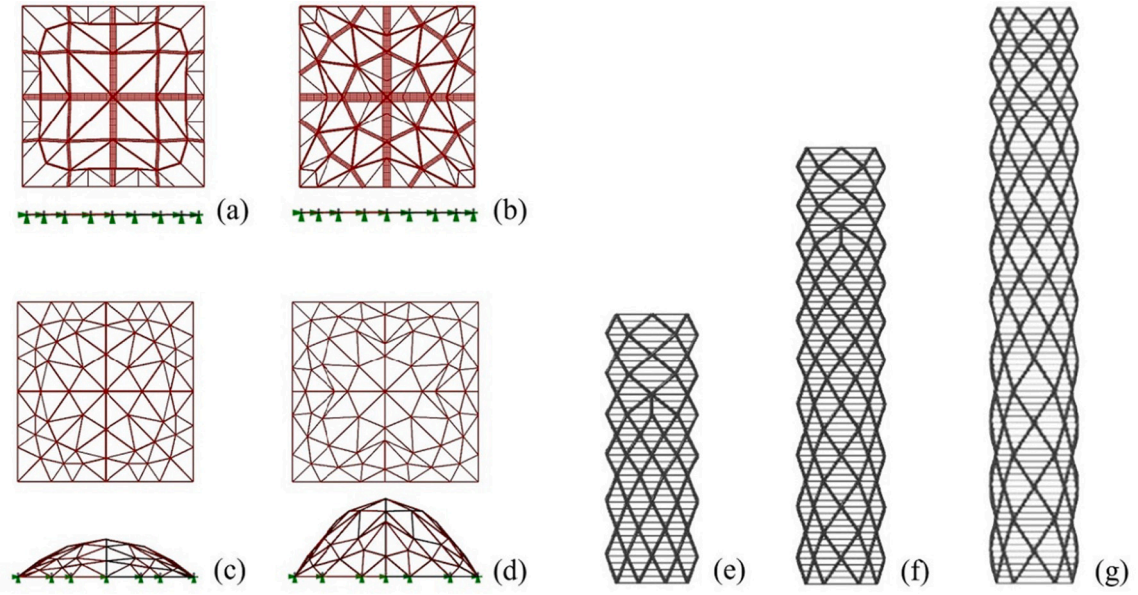

Fig. 9. TO patterns - grid shell (D_{lim} equal to B/250 and B/500): (a) H/B = 0 and q = 3.5 kN/m^2; (b) H/B = 0 and q = 10 kN/m^2; (c) H/B = 0.21; (d) H/B = 0.42; diagrid-like structure (D_{lim} = H/500): (e) H/B = 3, (f) H/B = 5; (g) H/B = 6.6.

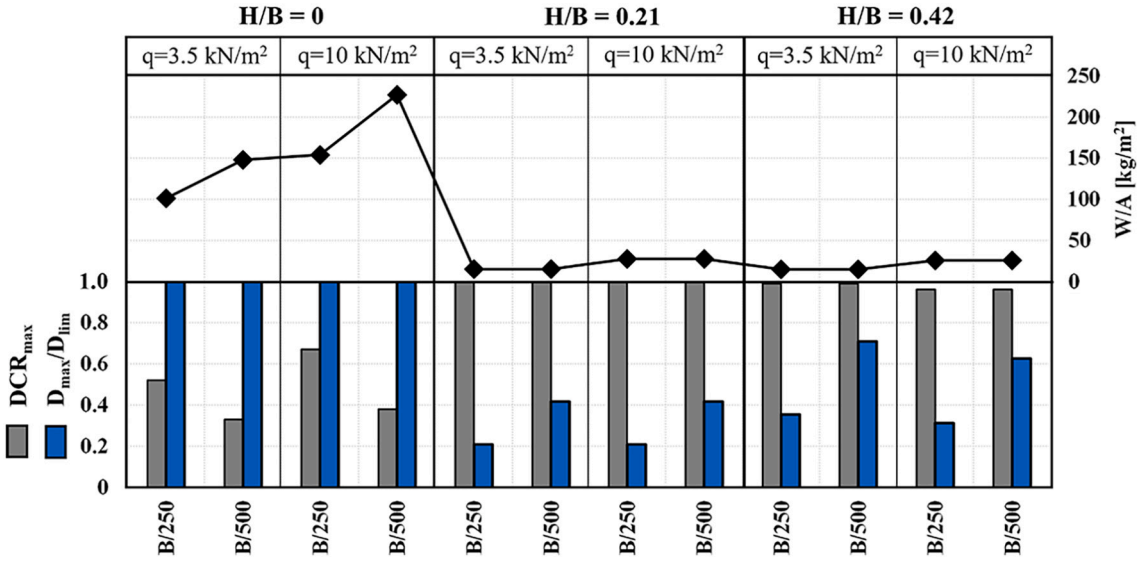

Fig. 10. Grid shells: performance assessment in terms of Weight, DCR and maximum Displacements.

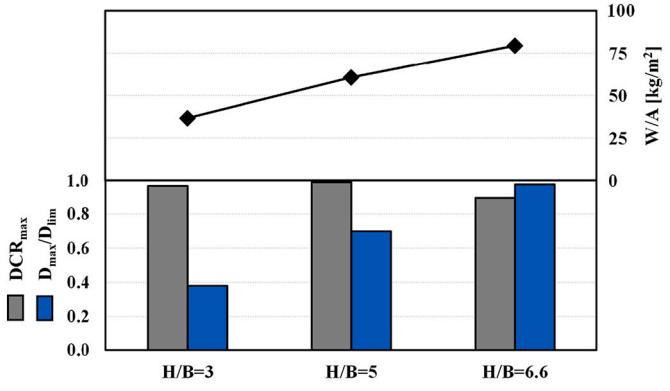

Fig. 11. Diagrids: optimized patterns and performance assessment in terms of Weight, DCR and maximum Displacements.

approach, provides advantages from the point of view of the structural weight, which is an indicative parameter of the cost of the structure.

The above results and observations confirm that the structural behaviour of grid shells is strongly affected by the rise to span ratio, while for the diagrid the aspect ratio has a similar importance. Nevertheless, the proposed structural grammar is able to find the optimal solutions, also when the structural behaviour changes.

A representation of the efficacy of the generative process, which drive the solutions toward the best one, is graphically provided in the parallel coordinates plots of Fig. 12. More in details, Fig. 12a refers to grid shells, and in particular to the case of H/B = 0.21 and q = 3.5 kN/m^2. By considering the normalized domain, in the graph are reported the distances of nodes of each generated solution (in ordinate) with respect the starting solution in the x and y directions $a_{x,i}$ and $a_{y,i}$. It is clear that the solutions of first generation covers the entire space of explorations (yellow lines), while the last generation is composed by similar individuals (blue lines), which cover a limited zone of the space of

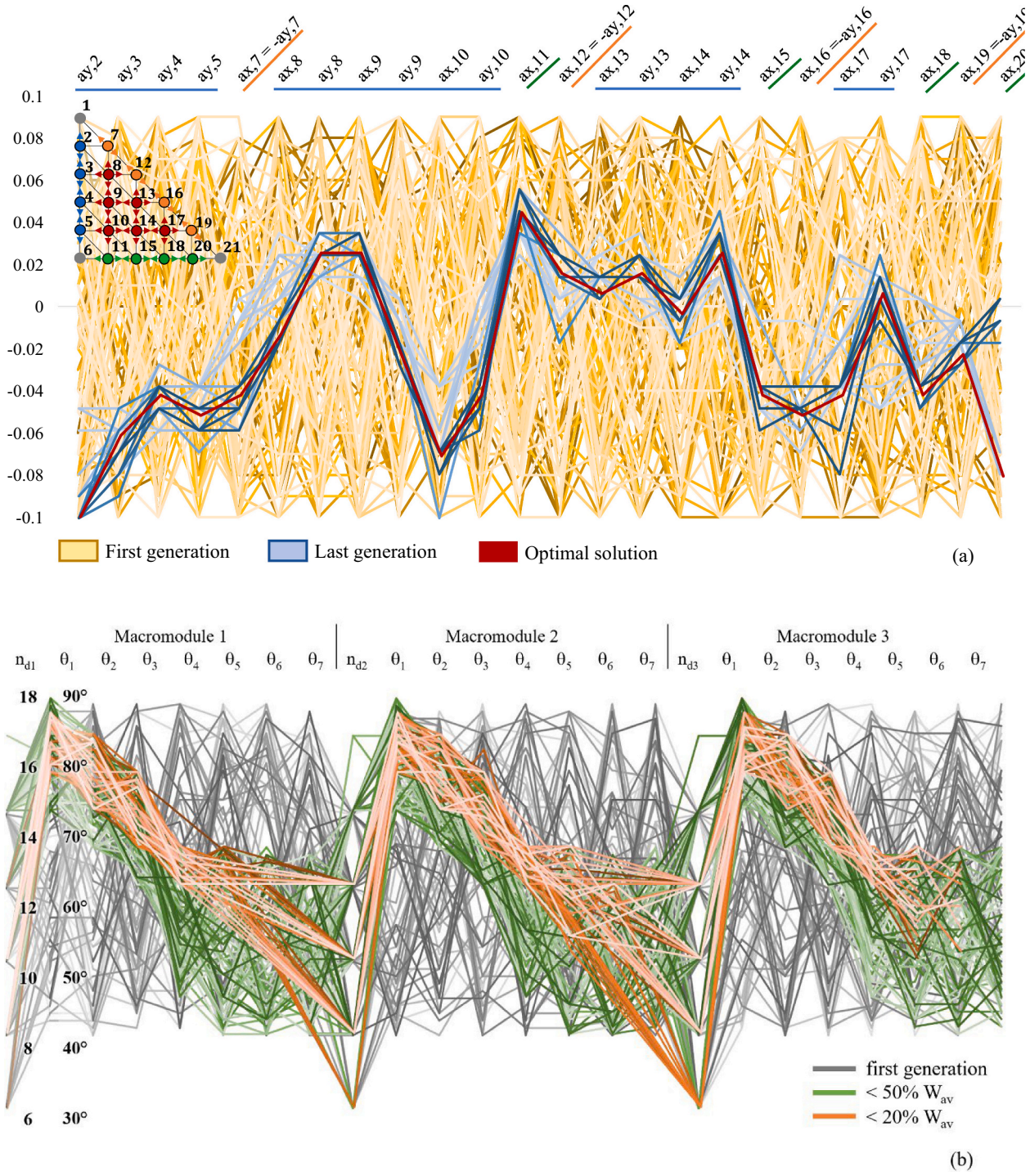

Fig. 12. Generative design: (a) grid shell, H/B = 0.21 and q = 3.5 kN/m^2; (b) diagrid-like structure, H/B = 6.6.

exploration around the solution characterized by the minimum weight (red line). It highlights the capacity of the algorithms to explore a multitude of solutions, and to drive the search toward the optimal one. Instead, Fig. 12b refers to the diagrid for the case of H/B = 6.6. Considering the *j-th* macro-module, the graph depicts the number n_{dj} of diagonals and the slope of the *k-th* diagonal, numbered from the external edge up to half width of the building façade. The solutions depicted with orange and green lines are characterized by a diagrid weight respectively <20% (orange lines) and 50% (green lines) of the average value W_{av}, evaluated considering all solutions (grey lines). It is also interesting to highlight that the values of θ_k reduces going from the outside to the inside of the half width of the building façade, accommodating the different demands of global forces, bending moment and shear, along the base, as found in the case of patterns inspired from isostatic lines [9].

6. Conclusions

The paper presents a structural grammar approach for the topology optimization of grid shell structures and diagrid tall buildings. The structural grammar is composed by three phases connected and interrelated each other: shape grammar; cross-section sizing and structural analysis; topology optimization process. The shape grammar is devoted

to the generation of different patterns, i.e. arrangements of structural members, through specifically designed rules that regulate the number, the density, and the slope of structural members. The phase of cross-section sizing is entrusted to an iterative process that assigns the smallest cross-sections able to satisfy the design requirements in terms of stiffness and strength, evaluated by means of a structural analysis. The topology optimization phase, based on genetic algorithms, aims to minimize the structural weight by varying the positions of the grid nodes, for the gridshell, and of the diagonals slope, for the diagrid, while satisfying the constraint conditions on stiffness and strength requirements. More in details, the topology is defined by the pattern of the structural members, generated by the shape grammar, that, in the case on grid shells and diagrids, assume a major role as it merges architectural/aesthetic features with structural/constructive requirements.

The proposed procedure has been applied to grid shells and diagrid tall buildings characterized by different rise-to-span ratios and aspect ratios, respectively. These two parameters strongly affect the structural behaviour and governing the design requirements. The results, presented in terms of structural weight and maximum value of Displacement and strength Demand to Capacity Ratios for each optimal solutions, show how the proposed structural grammar is able to generate optimal patterns according to the different behaviours and predominant design requirements of both grid shells and diagrids.

Further, the proposed shape grammar is able to create a huge number of structural patterns characterized by significant geometrical diversity; it could be combined with multi-objective optimization algorithms, in order to find a set of pareto-optimal solutions to be evaluated on the basis of different objective functions, not only concerning structural aspects, but also constructive, architectural and/or functional features. In this context, Tomei et al. [7] proposed a method for evaluating a complexity index for diagrids that takes into account constructability aspects, depending on: the number of joints, the number of different cross-sections, the number of splices required for the diagonals, the number of diagonals and the number of members with different lengths. A further development of the structural grammars could consist in assessing the generated solutions by multi-objective optimization algorithms with the aim to minimize both the weight and the complexity index. Alternatively, the optimization problem could be dealt with mono-objective optimization algorithms, but considering an objective function which takes into account different aspects, as the desirability function proposed in [38,70], that accounts for weight, lateral displacement, torsional rotation and complexity index. For the specific case of grid shells, in order to expand the procedure, it could be interesting to derive some considerations from previous works [9,54] which highlight the role of the joint rotational stiffness in the susceptibility to global buckling phenomena; in particular, optimization strategies are proposed to find the best position for a low number of rigid joints in hinged-joint grid shell, in order to obtain minimum weight solutions safe from global buckling phenomena [9,54]. By taking this in mind, it is possible to conceive a complexity index that also takes into account the number of rigid joints. The previous discussion emphasizes the “power” of merging generative design processes with optimization algorithms in the complex process finalized to the search of competitive solutions.

Declaration of Competing Interest

The authors declare that they have no known competing financial interests or personal relationships that could have appeared to influence the work reported in this paper.

Data availability

Data will be made available on request.

References

[1] A. Pugnale, T.M. Echenagucia, M. Sassone, Computational morphogenesis: design of freeform surfaces, in: Shell Structures for Architecture: Form Finding and Optimization, Routledge, 2014, pp. 225–236, https://doi.org/10.4324/9781315849270-28.

[2] M. Donofrio, Topology optimization and advanced manufacturing as a means for the design of sustainable buildings components, Procedia Engineering 145 (2016) 638–645, https://doi.org/10.1016/j.proeng.2016.04.054.

[3] A. Beghini, M. Sarkisian, Geometry optimization in structural design, in: Structural Engineers Association Of California 83rd Annual Convention Proceeding, 2014, pp. 153–164 (ISBN: 978-1-63439-886-2).

[4] M. Sarkisian, P. Lee, E. Long, D. Shook, Organic and natural forms in building design, in: Structures Congress 2010, American Society of Civil Engineers Structures, 2010, pp. 2840–2851, https://doi.org/10.1061/41130(369)257.

[5] L.L. Stromberg, A. Beghini, W.F. Baker, G.H. Paulino, Application of layout and topology optimization using pattern gradation for the conceptual design of buildings, Struct. Multidiscip. Optim. 43 (2011) 165–180, https://doi.org/10.1007/s00158-010-0563-1.

[6] L.L. Stromberg, A. Beghini, W.F. Baker, G.H. Paulino, Topology optimization for braced frames: combining continuum and beam/column elements, Eng. Struct. 37 (2012) 106–124, https://doi.org/10.1016/j.engstruct.2011.12.034.

[7] V. Tomei, M. Imbimbo, E. Mele, Optimization of structural patterns for tall buildings: the case of diagrid, Eng. Struct. 171 (2018), https://doi.org/10.1016/j.engstruct.2018.05.043, 280–197.

[8] E. Mele, M. Imbimbo, V. Tomei, The effect of slenderness on the design of diagrid structures, International Journal of High-Rise Buildings 8 (2019) 83–94, https://doi.org/10.21022/IJHRB.2019.8.2.83.

[9] E. Grande, M. Imbimbo, V. Tomei, Optimization strategies for grid shells: the role of joints, J. Archit. Eng. 26 (2020), https://doi.org/10.1061/(ASCE)AE.1943-5568.0000375.

[10] E. Grande, M. Imbimbo, V. Tomei, A Two-Stage Approach for the Design of Grid Shells, in: Structures and Architecture - Proceeding of 3rd International Conference of Structures & Architectures 2016, Taylor & Francis Group, 2016 (ISBN: 9781138026513).

[11] V. Tomei, E. Grande, M. Imbimbo, Influence of geometric imperfections on the efficacy of optimization approaches for grid-shells, Eng. Struct. 228 (2021), https://doi.org/10.1016/j.engstruct.2020.111502.

[12] V. Tomei, E. Grande, M. Imbimbo, Design optimization of gridshells equipped with pre-tensioned rods, Journal Of Building Engineering 52 (2022), https://doi.org/10.1016/J.JOBE.2022.104407.

[13] F. Cascone, D. Faiella, V. Tomei, E. Mele, Stress lines inspired structural patterns for tall buildings, Eng. Struct. 229 (2021), https://doi.org/10.1016/j.engstruct.2020.111546.

[14] I. Chatzikonstantinou, B. Ekici, I.S. Sariyildiz, B.K. Koyunbaba, Multi-objective diagrid façade optimization using differential evolution, in: 2015 IEEE Congress on Evolutionary Computation 2015 - Proceedings, Institute of Electrical and Electronics Engineers Inc., 2015, pp. 2311–2318, https://doi.org/10.1109/CEC.2015.7257170.

[15] L. Sgambi, K. Gkoumas, F. Bontempi, Genetic algorithms for the dependability assurance in the design of a long-span suspension bridge, Computer-Aided Civil and Infrastructure Engineering 27 (2012) 655–675, https://doi.org/10.1111/j.1467-8667.2012.00780.x.

[16] A.J. Torii, R.H. Lopez, F. Biondini, An approach to reliability-based shape and topology optimization of truss structures, Eng. Optim. 44 (2012) 37–53, https://doi.org/10.1080/0305215X.2011.558578.

[17] G. Quinn, Structural analysis for the pneumatic erection of elastic gridshells, Structures. 28 (2020) 2276–2290, https://doi.org/10.1016/j.istruc.2020.10.012.

[18] F. Biondini, F. Bontempi, P.G. Malerba, Fuzzy reliability analysis of concrete structures, Comput. Struct. 82 (2004) 1033–1052, https://doi.org/10.1016/j.compstruc.2004.03.011.

[19] D. Liu, P. Hao, K. Zhang, K. Tian, B. Wang, G. Li, et al., On the integrated design of curvilinearly grid-stiffened panel with non-uniform distribution and variable stiffener profile, Mater. Des. 190 (2020), 108556, https://doi.org/10.1016/J.MATDES.2020.108556.

[20] F. Cascone, D. Faiella, V. Tomei, E. Mele, A structural grammar approach for the generative design of diagrid-like structures, Buildings 11 (2021), https://doi.org/10.3390/BUILDINGS11030090.

[21] P.W. Christensen, A. Klarbring, An introduction to structural optimization, Solid Mechanics and its Applications 153 (2008) 1–220, https://doi.org/10.1007/978-1-4020-8666-3_1.

[22] G. Stiny, J. Gips, Shape grammars and the generative specification of painting and sculpture, in: O.R. Petrocelli (Ed.), The Best Computer Papers of 197, Auerbach, Philadelphia, 1972, pp. 125–135 (ISBN: 0877691274).

[23] G. Stiny, Introduction to shape and shape grammars, Environment and Planning B: Planning and Design 7 (1980) 343–351, https://doi.org/10.1068/b070343.

[24] K. Shea, Essays of Discrete Structures: Purposeful Design of Grammatical Structures by Directed Stochastic Search, Carnegie Mellon University, 1997, pp. 19–56. Ph.D Thesis, https://citeseerx.ist.psu.edu/viewdoc/summary?doi=10.1.1.709.4066 (latest access on 11 July 2022).

[25] K. Shea, J. Cagan, Languages and semantics of grammatical discrete structures, Artificial Intelligence for Engineering Design, Analysis and Manufacturing 13 (1999) 241–251, https://doi.org/10.1017/S0890060499134012.

[26] I. Mirtsopoulos, C. Fivet, Design space exploration through force-based grammar rule, ArchiDOCT. 8 (2020) 50–64. https://infoscience.epfl.ch/record/278332 (latest access on 6 November 6 2021).

[27] S. Boonstra, K. van der Blom, H. Hofmeyer, M.T.M. Emmerich, Conceptual structural system layouts via design response grammars and evolutionary algorithms, Autom. Constr. 116 (2020), https://doi.org/10.1016/J.AUTCON.2019.103009.

[28] I. Jowers, C. Earl, G. Stiny, Shapes, structures and shape grammar implementation, Comput. Aided Des. 111 (2019) 80–92, https://doi.org/10.1016/J.CAD.2019.02.001.

[29] L. Mandow, J.L. Pérez-de-la-Cruz, A.B. Rodríguez-Gavilán, M. Ruiz-Montiel, Architectural planning with shape grammars and reinforcement learning: habitability and energy efficiency, Eng. Appl. Artif. Intell. 96 (2020), https://doi.org/10.1016/J.ENGAPPAI.2020.103909.

[30] X. Wang, Y. Song, P. Tang, Generative urban design using shape grammar and block morphological analysis, Frontiers of Architectural Research 9 (2020) 914–924, https://doi.org/10.1016/J.FOAR.2020.09.001.

[31] Y. Yu, T.C.K. Hong, A. Economou, G.H. Paulino, Rethinking origami: a generative specification of origami patterns with shape grammars, Comput. Aided Des. 137 (2021), https://doi.org/10.1016/J.CAD.2021.103029.

[32] M.M. Ali, K.S. Moon, Structural developments in tall buildings: current trends and future prospects, Archit. Sci. Rev. 50 (2007) 205–223, https://doi.org/10.3763/asre.2007.5027.

[33] E. Mele, M. Toreno, G. Brandonisio, A. De Luca, Diagrid structures for tall buildings: case studies and design considerations, Structural Design of Tall and Special Buildings 23 (2014) 124–145, https://doi.org/10.1002/tal.1029.

[34] G. Angelucci, F. Mollaioli, R. Tardocchi, A new modular structural system for tall buildings based on tetrahedral configuration, Buildings. 10 (2020) 1–22, https://doi.org/10.3390/BUILDINGS10120240.

[35] M. Bruggi, Conceptual Design of Diagrids and Hexagrids by distribution of lattice structures, Frontiers in Built Environment 6 (2020), https://doi.org/10.3389/FBUIL.2020.00080.

[36] D. Scaramozzino, G. Lacidogna, A. Carpinteri, New trends towards enhanced structural efficiency and aesthetic potential in tall buildings: the case of diagrids, Applied Sciences (Switzerland) 10 (2020) 3917, https://doi.org/10.3390/APP10113917.

[37] V. Mohsenian, S. Padashpour, I. Hajirasouliha, Seismic reliability analysis and estimation of multilevel response modification factor for steel diagrid structural systems, Journal of Building Engineering 29 (2020), https://doi.org/10.1016/J.JOBE.2019.101168.

[38] D. Scaramozzino, B. Albitos, G. Lacidogna, A. Carpinteri, Selection of the optimal diagrid patterns in tall buildings within a multi-response framework: application of the desirability function, Journal Of Building Engineering (2022), https://doi.org/10.1016/J.JOBE.2022.104645.

[39] G. Lacidogna, G. Nitti, D. Scaramozzino, A. Carpinteri, Diagrid systems coupled with closed- and open-section shear walls: optimization of geometrical characteristics in tall buildings, Procedia Manufacturing 44 (2020) 402–409, https://doi.org/10.1016/J.PROMFG.2020.02.277.

[40] C. Liu, D. Fang, L. Zhao, J. Zhou, Seismic fragility estimates of steel diagrid structure with performance-based tests for high-rise buildings, Journal Of Building Engineering 52 (2022), https://doi.org/10.1016/J.JOBE.2022.104459.

[41] T. Orhan, K. Taşkın, Automated topology design of high-rise diagrid buildings by genetic algorithm optimization, Structural Design of Tall and Special Buildings 30 (2021), https://doi.org/10.1002/TAL.1853.

[42] F. Laccone, A. Casali, M. Sodano, M. Froli, Morphogenesis of a bundled tall building: biomimetic, structural, and wind-energy design of a multi-core-outrigger system combined with diagrid, Structural Design of Tall and Special Buildings 30 (2021), https://doi.org/10.1002/TAL.1839.

[43] B. Eilouti, Shape grammars as a reverse engineering method for the morphogenesis of architectural façade design, Frontiers of Architectural Research 8 (2019) 191–200, https://doi.org/10.1016/J.FOAR.2019.03.006.

[44] D. Scaramozzino, G. Lacidogna, Diagrid and Hexagrid structures: new perspectives in Design of Tall Buildings, The Open Construction & Building Technology Journal 15 (2022) 221–224, https://doi.org/10.2174/1874836802115010221.

[45] F.H. Alkhatib, N. Kasim, W.I. Goh, A.A.H. Al-Masudi, Multidisciplinary Computational Optimization: An Integrated Approach to Achieve Sustainability in Tall Building Design at Early Stage-Review, 2021 3rd International Sustainability and Resilience Conference: Climate Change, 2021, pp. 562–566, https://doi.org/10.1109/IEEECONF53624.2021.9668031.

[46] K.S. Moon, Optimal grid geometry of diagrid structures for tall buildings, Archit. Sci. Rev. 51 (2008) 239–251, https://doi.org/10.3763/asre.2008.5129.

[47] C. Zhang, F. Zhao, Y. Liu, Diagrid tube structures composed of straight diagonals with gradually varying angles, Structural Design of Tall and Special Buildings 21 (2012) 283–295, https://doi.org/10.1002/tal.596.

[48] G.M. Montuori, E. Mele, G. Brandonisio, A. De Luca, Geometrical patterns for diagrid buildings: exploring alternative design strategies from the structural point of view, Eng. Struct. 71 (2014) 112–127, https://doi.org/10.1016/j.engstruct.2014.04.017.

[49] J.N. Richardson, S. Adriaenssens, R. Filomeno Coelho, P. Bouillard, Coupled form-finding and grid optimization approach for single layer grid shells, Eng. Struct. 52 (2013) 230–239, https://doi.org/10.1016/j.engstruct.2013.02.017.

[50] R. Qiang Feng, F. Cheng Liu, W. Jia Xu, M. Ma, Y. Liu, Topology optimization method of lattice structures based on a genetic algorithm, International Journal of Steel Structures 16 (2016) 743–753, https://doi.org/10.1007/s13296-015-0208-8.

[51] J. Rombouts, G. Lombaert, L. De Laet, M. Schevenels, A novel shape optimization approach for strained gridshells: design and construction of a simply supported gridshell, Eng. Struct. 192 (2019) 166–180, https://doi.org/10.1016/j.engstruct.2019.04.101.

[52] R.Q. Feng, J.M. Ge, Shape optimization method of free-form cable-braced grid shells based on the translational surfaces technique, International Journal of Steel Structures 13 (2013) 435–444, https://doi.org/10.1007/s13296-013-3004-3.

[53] F. Cheng Liu, R. Qiang Feng, K.D. Tsavdaridis, G. Yan, Designing efficient grid structures considering structural imperfection sensitivity, Engineering Structures 204 (2020), https://doi.org/10.1016/j.engstruct.2019.109910.

[54] E. Grande, M. Imbimbo, V. Tomei, Role of global buckling in the optimization process of grid shells: design strategies, Eng. Struct. 156 (2018) 260–270, https://doi.org/10.1016/j.engstruct.2017.11.049.

[55] E. Grande, M. Imbimbo, V. Tomei, Structural optimization of grid shells: design parameters and combined strategies, J. Archit. Eng. 24 (2018), https://doi.org/10.1061/(ASCE)AE.1943-5568.0000286.

[56] W. Gythiel, M. Schevenels, Gradient-based size, shape, and topology optimization of single-layer reticulated shells subject to distributed loads, Struct. Multidiscip. Optim. 65 (2022) 1–18, https://doi.org/10.1007/S00158-022-03225-W.

[57] V. Tomei, E. Grande, M. Imbimbo, Influence of pretensioned rods on structural optimization of grid shells, in: Magd Abdel Wahab (Ed.), Proceedings of the 4th International Conference on Numerical Modelling in Engineering. Lecture Notes in Civil Engineering, Springer, Singapore, 2022, pp. 93–100, https://doi.org/10.1007/978-981-16-8185-1.

[58] Z. Li, J. Ye, B. Gao, Q. Wang, G. Quan, P. Shepherd, Digital and automatic design of free-form single-layer grid structures, Autom. Constr. 133 (2022), https://doi.org/10.1016/J.AUTCON.2021.104025.

[59] Q. Sheng Wang, J. Ye, H. Wu, B. Qing Gao, P. Shepherd, A triangular grid generation and optimization framework for the design of free-form gridshells, Computer-Aided Design 113 (2019) 96–113, https://doi.org/10.1016/J.CAD.2019.04.005.

[60] Z. Shan, L. Chen, Q. Wang, H. Wu, B. Gao, Simplified quadrilateral grid generation of complex free-form gridshells by surface fitting, Journal Of Building Engineering 48 (2022), https://doi.org/10.1016/J.JOBE.2021.103827.

[61] F. Venuti, Influence of pattern anisotropy on the structural behaviour of free-edge single-layer gridshells, Curved and Layered Structures 8 (2021) 119–129, https://doi.org/10.1515/cls-2021-0011.

[62] D.E. Goldberg, Genetic Algorithms in Search, Optimization and Machine Learning, Addison-Wesley Publishing Company, Inc., 1989 (ISBN:0201157675).

[63] D. Rutten, Grasshopper: Generative Modeling for Rhino. www.grasshopper3d.com, 2007 (latest access on 11 July 2022).

[64] R. McNeel, RHINOCEROS: NURBS modeling for Windows. www.rhino3d.com, 2017 (latest access on 11 July 2022).

[65] C. Preisinger, Karamba 3D. Parametric structural modeling, User Manual Version 1.3.1 (2018) 6–114. https://manual-1-3.karamba3d.com/ (latest access on 11 July 2022).

[66] C. Preisinger, Linking structure and parametric geometry, Archit. Des. 83 (2013) 110–113, https://doi.org/10.1002/ad.1564.

[67] European Committee for Standardization EN 1991-1-1:2010, Eurocode 1: Actions on Structures. https://www.phd.eng.br/wp-content/uploads/2015/12/en.1991.1.1.2002.pdf, 2010 (latest access on 11 July 2022).

[68] European Committee for Standardization, EN 1993–1-1, Eurocode 3: Design of Steel Structures—Part 1–1: General Rules and Rules for Buildings. https://www.phd.eng.br/wp-content/uploads/2015/12/en.1993.1.1.2005.pdf, 2005 (latest access on 11 July 2022).

[69] C. Preisinger, Karamba3D. www.karamba3d.com, 2019 (latest access on 11 July 2022).

[70] G. Lacidogna, D. Scaramozzino, A. Carpinteri, Optimization of diagrid geometry based on the desirability function approach, Curved and Layered Structures. 7 (2020) 139–152, https://doi.org/10.1515/CLS-2020-0011.